

Soft Scattering Re - Visited

Uri Maor*

Department of Particles Physics, School of Physics and Astronomy
Raymond and Beverly Sackler Faculty of Exact Science
Tel Aviv University, Tel Aviv 69978, Israel

An updated formulation of soft diffraction, compatible with s and t channel unitarity, is presented. Its consequent general soft scattering features at high energies are explored. The critical interplay between theory and data analysis and its consequent implications with regards to the theoretical foundations of soft scattering theory are discussed.

1 Introduction

The renewed interest in soft scattering and Pomeron physics, which was dormant for many years, can be traced to the market demand for reliable estimates of hard diffraction gap survival probabilities, notably diffractive Higgs production at the LHC. We note that the present vigorous study of this subject is essentially based on sophisticated utilization of relatively old theoretical ideas and models, such as Gribov's Reggeon field theory[1], Good and Walker (GW) decomposition of the proton wave function accounting for low mass diffraction[2] and the eikonal approximation[3] which secures the compatibility of the scattering amplitudes with s channel unitarity. Compliance with t channel unitarity is associated with multi Pomeron interactions (\mathbb{P} enhancement) which are a generalization of Mueller's triple Pomeron mechanism[4], provided $G_{3\mathbb{P}}$, the triple Pomeron coupling, is not too small. This mechanism supplements GW diffraction with an additional high mass diffraction.

In this talk I shall discuss the modeling and consequent soft scattering predictions derived from the above dynamical considerations. The implied gap survival probabilities will be discussed by Gotsman in the following talk. I shall assume a Regge like parametrization in which the \mathbb{P} is super critical, i.e. $\alpha_{\mathbb{P}}(t) = 1 + \Delta_{\mathbb{P}} + \alpha'_{\mathbb{P}}t$, where $\Delta_{\mathbb{P}} > 1$. The above \mathbb{P} exchange violates s -unitarity at high energies. Recall that implementing s -unitarity is model dependent. I shall confine myself to eikonal models which have the virtue of simplicity.

In the ISR-Tevatron range σ_{tot} and σ_{el} are well reproduced by Donnachie-Landshoff (DL) non screened Regge parametrization with $\Delta_{\mathbb{P}} = 0.08$ and $\alpha'_{\mathbb{P}} = 0.25 GeV^{-2}$. The energy dependence of the soft diffractive cross sections (notably σ_{sd}) is much milder, implying that strong screenings initiated by s -unitarity must be taken into account. As we shall see, the interplay between theory and data analysis results in strong constraints on both $\Delta_{\mathbb{P}}$ and $\alpha'_{\mathbb{P}}$ inputs. This results in profound consequences for the nature of the Pomeron and its QCD foundations, providing a unifying interpretation of soft and hard Pomerons.

*e-mail: maor@post.tau.ac.il

2 Good-Walker Eikonal Models

Consider a system of two Fock states, a hadron Ψ_h and a diffractive state Ψ_D which are orthonormal. The GW mechanism stems from the observation that these states do not diagonalize the 2x2 interaction matrix \mathbf{T} . Introduce two wave functions Ψ_1 and Ψ_2 which diagonalize \mathbf{T} ,

$$A_{i,k}^{i',k'} = \langle \Psi_i | \Psi_k | \mathbf{T} | \Psi_{i'} | \Psi_{k'} \rangle = A_{i,k} \delta_{i,i'} \delta_{k,k'}. \quad (1)$$

i.e. the $A_{i,k}$ amplitudes are constructed from the elastic scatterings of Ψ_i and Ψ_k . In this representation the observed hadronic states are written

$$\Psi_h = \alpha \Psi_1 + \beta \Psi_2 \quad \Psi_D = -\beta \Psi_1 + \alpha \Psi_2, \quad (2)$$

where $\alpha^2 + \beta^2 = 1$. The corresponding unitarity equations are

$$\text{Im } A_{i,k}^S(s, b) = |A_{i,k}^S(s, b)|^2 + G_{i,k}^{in}(s, b), \quad (3)$$

where $G_{i,k}^{in}$ is the summed probability for all non GW inelastic processes induced by an initial (i, k) state. A general solution of Eq.(3) can be written as

$$A_{i,k}^S(s, b) = i \left(1 - \exp \left(-\frac{\Omega_{i,k}^S(s, b)}{2} \right) \right), \quad (4)$$

$$G_{i,k}^{in}(s, b) = 1 - \exp(-\Omega_{i,k}^S(s, b)), \quad (5)$$

where $\Omega_{i,k}^S$ are arbitrary. In the eikonal approximation $\Omega_{i,k}^S$ are assumed to be real and determined by the Born (non screened) input. From Eq.(5) we deduce that the probability that the initial projectiles (i, k) reach the final LRG diffractive interaction unchanged, regardless of the initial state re-scatterings, is given by $P_{i,k}^S = \exp(-\Omega_{i,k}^S(s, b))$. In general, we have to consider four possible (i, k) elastic re-scattering options. For initial p - p (or \bar{p} - p) the two off diagonal amplitudes are equal, $A_{1,2}^S = A_{2,1}^S$. The corresponding elastic, SD and DD amplitudes are

$$a_{el}(s, b) = i \{ \alpha^4 A_{1,1}^S + 2\alpha^2 \beta^2 A_{1,2}^S + \beta^4 A_{2,2}^S \}, \quad (6)$$

$$a_{sd}(s, b) = i \alpha \beta \{ -\alpha^2 A_{1,1}^S + (\alpha^2 - \beta^2) A_{1,2}^S + \beta^2 A_{2,2}^S \}, \quad (7)$$

$$a_{dd} = i \alpha^2 \beta^2 \{ A_{1,1}^S - 2A_{1,2}^S + A_{2,2}^S \}. \quad (8)$$

The GW mechanism was originally conceived so as to describe a system of a nucleon plus its diffractive N^* isobars. Obviously, this simplistic approach is not suitable for high energy diffraction where M_{diff}^2 is bounded by $0.05s^1$, implying a continua of diffractive Fock states. Throughout this talk I shall relate to GLMM[5] and KMR[6] models which are conceptually very similar, but differ significantly in both their formalism and data analysis. In the present context, two procedures were devised to overcome the above difficulty: GLMM lump together all GW diffractive states to an effective $|D\rangle$ state, to which we add the non GW \mathcal{P} enhanced high mass diffraction. In this approach the GW contribution is very significant and the mass distribution is smooth. KMR and LKMR[7] chose to confine GW diffraction to low $M_{diff}^2 < 10\text{GeV}^2$, to

¹this is an arbitrary bound commonly used.

which they add the high mass \mathbb{P} enhanced contribution. In this approximation the bulk of the diffractive mass is non GW, and its smoothness at 10GeV^2 is not secured.

GLMM, KMR and LKMR are multi channel eikonal models in which the initial re-scatterings of the incoming projectiles includes also diffractive states.

$$\Omega_{i,k}^S(s, b) = \nu_{i,k}^S(s) \Gamma_{i,k}^S(s, b, \dots), \quad (9)$$

where $\nu_{i,k}^S(s) = g_i g_k (\frac{s}{s_0})^{\Delta_{\mathbb{P}}}$ and $\Gamma_{i,k}^S$ are the b -space profiles. The profiles are external information in as much as, beside their normalization and asymptotic constraints on their behavior, they are determined by the data analysis. In GLMM $\Gamma_{i,k}^S$ are given as the b -transform of a two t -poles expression ($t = -q^2$). Setting $\alpha'_{\mathbb{P}}=0$, the profiles are energy independent

$$\frac{1}{(1 + q^2/m_i^2)^2} \times \frac{1}{(1 + q^2/m_k^2)^2} \implies \Gamma^S(b; m_i, m_k; \alpha'_{\mathbb{P}} = 0). \quad (10)$$

GLMM introduce a small energy dependence

$$m_i^2 \implies m_i^2(s) \equiv \frac{m_i^2}{1 + 4m_i^2 \alpha'_{\mathbb{P}} \ln(s/s_0)}. \quad (11)$$

The above parametrization is compatible with the requirements of analyticity/crossing symmetry at large b , pQCD at large q^2 and Regge at small q^2 . For details see Ref.[5]. KMR and LKMR use a different parametrization for $\Gamma_{i,k}^S$ which is numerically compatible with GLMM. The 3 groups reproduce $d\sigma_{el}/dt$ well in the forward $t < 0.5\text{GeV}^2$ cone.

Consider a model in which diffraction is exclusively GW. This was recently explicitly considered by GLMM and LKMR and non explicitly by KMR. These, as well as earlier GW models, fit the (different) elastic sectors of their data bases, obtaining output fitted $\Delta_{\mathbb{P}} = 0.10 - 0.12$ with $\chi^2/d.o.f. < 1.0$. The above GW models fail to reproduce the diffractive sectors of their data base. This deficiency is traced to the need to add the enhanced \mathbb{P} high mass contributions. This has been done in GLMM and KMR. LKMR enhanced \mathbb{P} input is confined to Eq.(12).

3 Multi Pomeron Interactions

Consider a single diffraction channel $p + p \rightarrow p + M_{sd}$. Mueller's triple Pomeron mechanism, derived from 3 body unitarity, leads to high SD mass which is non GW. In the leading order

$$M_{sd}^2 \frac{d\sigma^{3\mathbb{P}}}{dt dM_{sd}^2} = \frac{1}{16\pi^2} g_p^2(t) g_p(0) G_{3\mathbb{P}}(t) \left(\frac{s}{M_{sd}^2} \right)^{2\Delta_{\mathbb{P}} + 2\alpha'_{\mathbb{P}} t} \left(\frac{M_{sd}^2}{s_0} \right)^{\Delta_{\mathbb{P}}}. \quad (12)$$

The virtue of Eq.(12) is that $\Delta_{\mathbb{P}}$ can be determined from either the energy or mass dependences of the SD cross sections. This approximation is valid for $s \gg M_{sd}^2 \gg m_p$.

CDF analysis suggests[8] a relatively large value of $G_{3\mathbb{P}}$. Consequently, we need to consider a very large family of multi Pomeron interactions (enhanced \mathbb{P}) which are not included in the GW mechanism. As we shall see, this "new" dynamical feature initiates profound differences in the calculated values of soft cross sections and non GW diffractive gap survival probabilities (soft and hard). Note that this features become significant above the Tevatron energy.

GLMM and KMR treatment of \mathbb{P} enhanced interactions stems from Gribov classical Reggeon calculus [1] and Kaidalov et al.[9]. Recall that in this context the soft Pomeron is a simple pole in the J-plane, while the hard (BFKL) Pomeron is a branch cut. KMR model, which is a partonic model, derives directly from these sources. Its summation is confined to semi enhanced \mathbb{P} diagrams (see Fig.1b). KMR calculations are based on two ad hoc assumptions:

- 1) The coupling of a multi \mathbb{P} point vertex $n\mathbb{P} \rightarrow m\mathbb{P}$ ($n + m > 2$) is $g_m^n = \frac{1}{2}g_N n m \lambda^{n+m-2}$. In this notation $G_{3\mathbb{P}} = \lambda g_N$. Note that in Kaidalov et al. $g_m^n = \frac{1}{2}g_N \lambda^{n+m-2}$.
- 2) Most of LHC non GW diffractive reactions of interest are hard. Given a $3\mathbb{P}$ vertex, $G_{3\mathbb{P}}$ is unchanged by the interchange of soft and hard Pomerons. This is not self evident. A possible support for the above is obtained from GLMM interpretation of the Pomeron (see below).

As we shall see in the next chapter, the data analysis executed by GLMM and KMR converges to compatible exceedingly small $\alpha'_{\mathbb{P}}$ values and high, BFKL like, $\Delta_{\mathbb{P}} \simeq 0.30 - 0.35$. The adjustments of these parameters are correlated. In non screened Regge model $\Delta_{\mathbb{P}}$ controls the elastic cross section energy dependence, while $\alpha'_{\mathbb{P}}$ controls the energy dependence of the (shrinking) elastic slope. As $\alpha'_{\mathbb{P}}$ gets smaller $\Delta_{\mathbb{P}}$ becomes larger initiating stronger screening which compensates the reduction of $\alpha'_{\mathbb{P}}$, and vice versa. As we saw the vanishing value of the fitted $\alpha'_{\mathbb{P}}$ was explicitly dictated by the b-profiles GLMM and KMR chose. Non explicitly this choice initiated also the high $\Delta_{\mathbb{P}}$ fitted value. These results have profound implications:

- 1) A key observation of GLMM is that the exceedingly small fitted value of $\alpha'_{\mathbb{P}}$ implies that the "soft" \mathbb{P} is hard enough to be treated perturbatively. Following Gribov we identify the correlation between $\alpha'_{\mathbb{P}}$ and $\langle p_t \rangle$, the mean transverse momentum of the partons (actually, color dipoles) associated with the \mathbb{P} . $\langle p_t \rangle = 1/\sqrt{\alpha'_{\mathbb{P}}}$, from which we deduce that the QCD running coupling constant $\alpha_S \ll 1$. Accordingly, we proceed from Gribov's parton model interpretation to pQCD. GLMM sum over the enhanced diagrams. Technically, we have adopted the MPSI procedure[10] in which g_m^n is reduced to a sequence of triple \mathbb{P} vertexes (Fan diagrams). For details see Ref.[5]. This may pose a problem for the calculation of SD cross section for which the lowest order diagram is semi enhanced. To avoid this problem we have added to this calculation a term by term summation of the relevant semi enhanced diagrams.

- 2) The fitted high value of $\Delta_{\mathbb{P}}$ initiates strong screening which results in a renormalization of the Pomeron exchange amplitudes. As a result $\Delta_{\mathbb{P}}^{eff}$ is reduced monotonically with energy. In GLMM calculations $\Delta_{\mathbb{P}}^{eff}(2TeV) \simeq 0.070$, $\Delta_{\mathbb{P}}^{eff}(14TeV) \simeq 0.045$ and $\Delta_{\mathbb{P}}^{eff}(60TeV) \simeq 0.032$. KMR results are compatible with ours, see Table 2. The slow decrease of $\Delta_{\mathbb{P}}^{eff}$ raises the question if its value may become negative at high enough energies, larger than $W = 10^5 GeV$ which is the bound of validity of both GLMM and KMR. In GLMM we have checked that $\Delta_{\mathbb{P}}^{eff}(100TeV) > 0$. I am less clear about KMR. The compatibility between GLMM and KMR is surprising. As noted, GLMM sum over the enhanced diagrams (Fig.1a) while KMR sum over the semi enhanced diagrams (Fig.1b). Very intuitively (at the risk of being wrong), it seems that GLMM renormalize the \mathbb{P} propagator while KMR renormalize the \mathbb{P} vertex. A complete calculation should, obviously, include both contributions.

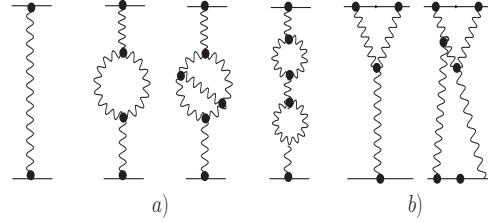


Figure 1: Low order terms of the Pomeron Green's function. a) Enhanced. b) Semi-enhanced.

4 The Interplay Between Theory and Data Analysis

The goal of the data analysis of interest is to adjust a set of theoretical parameters. To this end we construct:

- 1) A suitable data base adjusted, with a satisfactory resolution, to fix the parameters.
- 2) An adjustment procedure, be it a fit (GLMM, LKMR) or tuning by trial and error (KMR). We distinguish between a parameter adjustment which is executed through a reconstruction of the entire data base in one step (GLMM), and a sequence of factorizable adjustment steps (KMR, LKMR), each adjusting a sub group of the free parameters.

There is a significant difference between the data analysis carried out by GLMM and KMR. This reflects both in the choices of data bases made by the two groups and their adjustment procedures. The starting point of both investigations is the observation that a GW model reproduces the elastic data well, but its reproduction of the diffractive sector is deficient. Both groups claim to achieve an improved reproduction of their over all data base once the contributions of enhanced Pomeron diagrams are included.

GLMM have constructed a global data base so as to fit the multitude of free parameters. It includes σ_{tot} , σ_{el} , σ_{sd} , σ_{dd} and B_{el} in the ISR-Tevatron range, CDF differential elastic cross sections and SD mass distribution were checked for consistency. The conceptual approach of KMR and LKMR is completely different. Their data base contains only the measured values of $d\sigma_{el}/dt$, which enables to predict σ_{tot} , and $d\sigma_{sd}/dtd(M_{sd}^2/s)$. In my opinion KMR data base is too limited to enable a substantiation of their goals. Specifically:

- 1) As we saw, the b -profiles $\Gamma_{i,k}^S$ control the features of $d\sigma_{el}/dt$ which are only weakly coupled to the proposed dynamics. Indeed, 6 models, published over the last 10 years (3 KMR+LKMR+2 GLMM) with different dynamics, i.e., exclusive GW (GLMM, LKMR), GW+zero order \mathbb{P} enhancement (LKMR) and GW+ \mathbb{P} enhancement (GLMM, KMR). The output parameters spread over $0.1 \leq \Delta_{\mathbb{P}} \leq 0.55$ and $0 \leq \alpha'_{\mathbb{P}} \leq 0.066$. All 6 models reproduce, almost identically, the CDF distributions of $d\sigma_{el}/dt$. The unavoidable conclusion is that a reconstruction of $d\sigma_{el}/dt$ on its own has no resolution power. The only common ingredient to all 6 models is their compatible b -profiles. These profiles constrain $\alpha'_{\mathbb{P}}$ to very small values. This is the key observation leading to a pQCD (GLMM) or partonic (KMR) \mathbb{P} interpretation.
- 2) The reconstruction of CDF $d\sigma_{sd}/dtd(M_{sd}^2/s)$ by GLMM, LKMR and KMR partially substantiates the introduction of high mass multi Pomeron interactions. In my opinion, this investigation, in its present state, is unable to provide a decisive verdict on this issue. GLMM and KMR sum different sectors of the enhanced diagrams. LKMR take into account only the lowest order Mueller's $3\mathbb{P}$ diagram. Regardless of these differences, the three groups produce compatible output results which indicate that CDF data, as is, is not sufficient to differentiate between different modes of \mathbb{P} enhanced diagram summations.
- 3) To further clarify the experimental limitations, let us recall that CDF define their high mass diffraction bound $1 - x_L = \frac{M_{sd}^2}{s} \leq 0.15$ (the common bound is 0.05). KMR and LKMR define a lower bound $M_{sd}^2 > 10GeV^2$ which corresponds to $1 - x_L = 3 \cdot 10^{-6}$. Note that CDF SD mass distribution available for analysis corresponds to $1 - x_L > 2 \cdot 10^{-3}$. This mass distribution covers less than 20% of KMR expected high diffractive mass. GLMM have a completely different classification in which the GW low mass diffraction reduces monotonically with no arbitrary upper bound and the high mass is defined above $10GeV^2$, identical to KMR. Additional difficulties with the analysis of CDF data with $1 - x_L > 0.02$ is that an arbitrary significant background contribution has to be added. It is induced by secondary Regge diagrams such as $\mathbb{P}PR$. An

added element of ambiguity is that LKMR with a zero order $3\mathbb{P}$ calculation is faring as well as the high order summations of GLMM and KMR.

	$\Delta_{\mathbb{P}}$	β	$\alpha'_{\mathbb{P}}$ GeV^{-2}	g_1 GeV^{-1}	g_2 GeV^{-1}	m_1 GeV	m_2 GeV	$\chi^2/d.o.f.$
GW	0.120	0.46	0.012	1.27	3.33	0.913	0.98	0.87
GW+ \mathbb{P} - <i>enh.</i>	0.335	0.34	0.010	5.82	239.6	1.54	3.06	1.00

Table 1: Fitted parameters for GLMM GW and GW+ \mathbb{P} -enhanced models.

GLMM fitting procedure aims to reproduce our global data base. A fit with a GW model (no \mathbb{P} -enh) provides excellent reproduction of our elastic sector while the reproduction of the diffractive sector is very poor! The repeated fit with a GW+ \mathbb{P} -enh model results with a very good χ^2 . The outputs of both models are presented in Table 1. Checking we note that the exceedingly small value of $\alpha'_{\mathbb{P}}$ is persistently obtained in both models. The outputs of $\Delta_{\mathbb{P}}$ and g_2 change drastically once \mathbb{P} -enh is included. As we shall see this has significant consequences for the approach of $a_{el}(s, b)$ toward the black disc bound. As we have noted, KMR and LKMR tune g_1 and g_2 through a reproduction of $d\sigma_{el}/dt$ and the other parameters through a reproduction of $d\sigma_{sd}/dtd(M_{sd}^2/s)$. The values they obtain for $\Delta_{\mathbb{P}}$ and $\alpha'_{\mathbb{P}}$ are compatible with ours.

	Tevatron			LHC			W=10 ⁵ GeV		
	GLMM	KMR(07)	KMR(08)	GLMM	KMR(07)	KMR(08)	GLMM	KMR(07)	KMR(08)
σ_{tot}	73.3	74.0	73.7	92.1	88.0	91.7	108.0	98.0	108.0
σ_{el}	16.3	16.3	16.4	20.9	20.1	21.5	24.0	22.9	26.2
σ_{sd}	9.8	10.9	13.8	11.8	13.3	19.0	14.4	15.7	24.2
σ_{dd}	5.4	7.2		6.1	13.4		6.3	17.3	

Table 2: Comparison of GLMM, KMR(07) and KMR(08) cross sections in mb .

GLMM and KMR high energy Tevatron, LHC and Cosmic Rays predicted cross sections are summarized in Table 2. The elastic and total cross section outputs of the two models are compatible and, above the Tevatron, significantly lower than those obtained in models with no multi-Pomeron contributions. This is a consequence of $\Delta_{\mathbb{P}}$ renormalization due to the enhanced \mathbb{P} contributions. GLMM and KMR(07) predicted σ_{sd} are compatible, where KMR(07) are consistently larger by approximately 12%. KMR(08) predicted σ_{sd} are considerably larger than GLMM and are growing at a faster rate. The difference between KMR(07) and GLMM σ_{dd} predictions is even more dramatic, where $\sigma_{dd}(KMR(07))/\sigma_{dd}(GLMM) \simeq 3$ at $W = 10^5 GeV$. This very large difference is due to KMR large diffractive high mass predictions (see Table 2). The recent KMR(08) neglects to mention the high diffractive mass sector of double diffraction while showing higher SD cross sections than in KMR(07).

In my opinion the GLMM and KMR compatible predictions of total and elastic cross sections at the LHC and AUGER are of fundamental importance because they are significantly lower than the predicted values based on unitarity models with no \mathbb{P} enhancement. These measurements may provide a decisive support for the importance of multi-Pomeron interactions at high enough energies and, consequently, imply that the growth of the total and elastic cross

sections with energy is much more moderate than anticipated. This feature reflects in the slow decrease of Δ_P^{eff} shown in Sec 3.

5 The Approach Toward the Black Disc Bound

The GW base amplitudes of GLMM are $A_{i,k}^S$, with b dependences specified in Eq. (10) - Eq. (11). These are the building blocks with which we construct a_{el} , a_{sd} and a_{dd} (Eq. (6) - Eq. (8)). The $A_{i,k}^S$ amplitudes are bounded by the black disc unitarity limit of unity. Checking GLMM fitted parameters, presented in Table 1, we observe that g_1 and g_2 , which are comparable in the GW model, significantly change in the GW+ P enhanced model where we obtain $g_2 \gg g_1$. The implication of our fitted values of g_1 and g_2 , is that including the diffractive data in our global fit forces a large inequality between the three GW $A_{i,k}^S$ components. $A_{2,2}^S(s, b=0)$ reaches unity at a very low energy, $A_{1,2}^S(s, b=0)$ reaches unity at approximately $W=100\text{GeV}$ and $A_{1,1}^S(s, b=0)$ reaches unity at exceedingly high energies, well above LHC. The observation that one, or even two, of our $A_{i,k}^S(s, b)=1$ does not imply that the elastic scattering amplitude has reached the unitarity bound at these (s, b) values. $a_{el}(s, b)$ reaches the black disc bound when, and only when, $A_{1,1}^S(s, b)=A_{1,2}^S(s, b)=A_{2,2}^S(s, b)=1$, independent of β . The approach of $a_{el}(s, b=0)$ toward the black bound depends on the rate of $A_{1,1}^S(s, b)$ increase. This rate is very slow because of the relative smallness of g_1 to which we add that $A_{1,1}^S$ increase with energy above LHC becomes ever so moderate as a consequence of the renormalization reduction of Δ_P . Our results are different from the predictions of most available models, notably KMR, in which $a_{el}(s, b=0)$ reaches unity a few TeV above LHC. Note, though, that GLMM is the only model which includes the diffractive along side the elastic data in its data analysis. All models which predict saturation of $a_{el}(s, b=0)$ just above LHC have confined their data analysis exclusively to the elastic sector.

A consequence of the input $\Omega_{i,k}^S$ being very large at small b , is that $P_{i,k}^S(s, b)$ is exceedingly small at these small b values. As a result, given a diffractive (non screened) input, its output (screened) amplitude is peripheral in b . This is a general feature, common to all eikonal models regardless of their b -profiles details. The general behavior indicated above becomes more extreme at ultra high energies, where a_{el} continues to get darker and expand. Consequently, the inelastic diffractive channels (soft and hard) becomes more and more peripheral and relatively smaller when compared with the elastic channel. Given (s, b) at which $a_{el}(s, b) = 1$, the corresponding diffractive amplitudes, GW and non GW, vanish.

The behavior of the ratio $R_D = (\sigma_{el} + \sigma_{sd} + \sigma_{dd})/\sigma_{tot}$ conveys information regarding the onset of s-unitarity at very high energies. Assuming diffraction to be exclusively GW, we obtain[11] $R_D \leq 0.5$. Multi P induced diffraction is not included in R_D since it originates from $G_{i,k}^{in}$. Hence their non screened high mass cross section is suppressed by its survival probability which decreases with energy. In GLMM $R_D < 0.5$, decreasing slowly. In KMR(07) $R_D > 0.5$, increasing slowly with energy. The partial information available on KMR(08) suggests that its R_D grows even faster.

6 Conclusions

This presentation centered on the phenomenology implied by multi Pomeron dynamics incorporated in soft diffraction and its consequences on soft scattering.

The concept of \mathbb{P} enhancement was triggered, at the time, by the assessment that $G_{3\mathbb{P}}$ is not too small. Our view of the Pomeron got more focused with the updated data analysis of soft scattering in which we get $\Delta_{\mathbb{P}} \simeq 0.30 - 0.35$ and $\alpha'_{\mathbb{P}} \simeq 0.01$. The implied KMR Pomeron is hard enough to be treated partonically, in which the traditional classification of the soft \mathbb{P} as a simple J-pole and the hard \mathbb{P} as a branch cut in the J-plane is maintained. GLMM went further on identifying the soft \mathbb{P} with the hard \mathbb{P} . This is, clearly, a fundamental theoretical issue which should be further investigated.

As it stands this dynamics is compatible with the data, but at present we can not support it with a decisive verification. A prediction shared by GLMM and KMR is the expected significant reduction, compared with non screened predictions, of σ_{tot} and σ_{el} at the LHC. In my opinion this measurment is of a critical value.

Decisive experimental signatures of \mathbb{P} -enh are expected, essentially, above the Tevatron. Consequently, we should be prudent when evaluating phenomenological models which reproduce the Tevatron data well. This is, obviously, required of a successful model, but is definitely not sufficient.

7 Acknowledgments

This research was supported in part by BSF grant # 20004019 and by a grant from Israel Ministry of Science and the Foundation for Basic Research of the Russian Federation.

References

- [1] V.A. Gribov: *Sov. J. Nuclear Phys.* **9** 369 (1969), arXiv:hep-ph/0006158, *Gauge Theories and Quark Confinement* PHASIS, Moscow (2002)
- [2] M.L. Good and W.D. Walker: *Phys. Rev.* **120** 1857 (1960).
- [3] R.J. Glauber: In *Lectures in Theoretical Physics Vol I*, ed. W.E. Brittin and L.G. Dunham, Interscience Pub., London 1959.
- [4] A.H. Mueller: *Phys. Rev.* **D2** 2963 (1970), **D2** 150 (1971).
- [5] E. Gotsman, E. Levin, U. Maor and J.S. Miller: *Eur. Phys. J.* **C57** 269 (2008), arXiv: 0901.1540[hep-ph], arXiv: 0903.0247[hep-ph].
- [6] M.G. Ryskin, A.D. Martin and V.A. Khoze: *Eur. Phys. J.* **C54** 199 (2008)(GLM07), *Eur. Phys. J.* **C60** 249 (2009), arXiv:0811.1481[hep-ph], arXiv:0811.4571[hep-ph], arXiv:0812.2413[hep-ph](GLM08).
- [7] E.G. Luna, V.A. Khoze, A.D. Martin and M.G. Ryskin: *Eur. Phys. J.* **C59** 1 (2009).
- [8] CDF Collaboration: *Phys. Rev.* **D50** 5535 (1994); K. Goulianos and J. Montanha: *Phys. Rev.* **D59** 114017 (1999).
- [9] A.B. Kaidalov, L.A. Ponomarev and K.A. Ter-Martirosyan: *Sov. J. Nucl. Phys.* **44** 468 (1986).
- [10] A. H. Mueller and B. Patel: *Nucl. Phys.* **B425** 471 (1994); A. H. Mueller and G. P. Salam: *Nucl. Phys.* **B475** 293 (1996); G. P. Salam: *Nucl. Phys.* **B461** 512 (1996); E. Iancu and A. H. Mueller: *Nucl. Phys.* **A730** 460 (2004), *Nucl. Phys.* **A730** 494 (2004).
- [11] J. Pumplin: *Phys. Rev.* **D8** 2 (1973).